Research on Seismic Performance of Corrugated Steel Plate Shear Walls with Inelastic Buckling Subjected to Lateral Loads

Qiang Cao[1] · Jingyu Huang[2,3] · Dongzhou Wang[2] · Liang Zhao[2] · Zhewei Wu[2]

Abstract

The corrugated steel plate shear wall (CSPSW) with inelastic buckling of a corrugated steel plate (CSP) could restrict the elastic out-of-plane buckling of in-filled steel plates with appropriate CSPs, and lateral displacement could be restricted in the structures. So, the CSPSWs with inelastic buckling of CSPs could be applicable in high buildings or the structures with strict requirements of lateral displacement. This paper presents the research works on the seismic behaviour of the CSPSW with inelastic buckling of a corrugated steel plate. A numerical model was developed to simulate the seismic performance of the CSPSW with the inelastic buckling of the CSP, and the FE model was validated through experiment. Subsequently, parametric analyses were performed to investigate for the effects of those key parameters on the seismic behaviour of CSPSWs, such as the height—thickness ratio, aspect ratio, horizontal panel width, corrugation angle, initial imperfections, and surrounding frame stiffness. The buckling and post buckling behaviour, failure modes, ductility and energy absorption capacity of the shear walls were discussed. The results reveal that the CSPSW show high strength, better ductility, and stable hysteretic characteristics. The failure modes of the CSPSWs with CSPs inelastic buckling are the failure of the tension field strips along the along the diagonals in the whole CSPs. And the corners of CSPs in CSPs are weak parts, which should be strengthened in future designs. Besides these, the surrounding frame stiffness should be greater than $I_{c\,min}$ to ensure energy-dissipating capacity and buckling capacity stability of CSPSWs.

Keywords Corrugated steel plate shear wall · Seismic performance · Failure mode · Tension field action · Inelastic buckling

Abbreviations

a	Inclined panel width
b	Horizontal panel width of corrugated plate
B	Corrugated steel plate width
b_s	Centre-to-centre distance of adjacent columns
c	Horizontal length of single wave of corrugated plate
d	Horizontal projection of the inclined panel width
d_r	Corrugation depth
E	Young's modulus of corrugated steel plate material
h_r	Corrugation depth
H	Height of corrugated plate
$I_{c\,min}$	Minimum value of surrounding frame stiffness
I_f	Section moment of inertia of frame
s	Length single wave of corrugated plate
t_w	Thickness of corrugated plate
θ	Corrugation angle of corrugated plate
α	Inclination angle of tension field in corrugated steel plate
λ	Height–thickness ratio of CSPSW

✉ Jingyu Huang
  huangjingyu@tongji.edu.cn

1 College of Transportation Engineering, Tongji University, Shanghai 201804, China

2 College of Civil Engineering, Tongji University, 1239 Siping Road, Shanghai 200092, China

3 National Maglev Transportation Engineering R&D Center, Tongji University, Shanghai 201804, China

1 Introduction

As a new alternative lateral force resisting system (Cao et al., 2016; Gholizadeh & Yadollahi, 2012; Hosseinzadeh & Aziminejad, 2017; Zhao et al., 2017), a corrugated steel plate shear wall (CSPSW) possesses enhanced in-plane and out-of-plane stiffness, high strength, ductility, and stable hysteretic characteristics owing to the excellent cross-sectional characteristics of its CSP, as shown in Fig. 1. The CSPSW with inelastic buckling of CSPs could restrict the elastic out-of-plane buckling of in-filled steel plates with appropriate
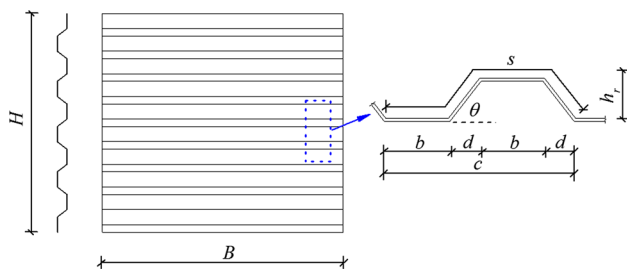
Fig. 1 Profile of a CSP

Fig. 2 Configuration of a CSPSW

CSPs at a low cost (Cao & Huang, 2018; Driver et al., 2006; Easley & ASCE., 1969; Yi et al., 2008), and lateral displacement could be restricted in the structures used the shear walls as the lateral resisting systems. So, the CSPSWs with inelastic buckling of CSPs could be applicable in high buildings or the structures with strict requirements of lateral displacement. So, it is necessary to investigate the seismic behaviour of the CSPSWs with inelastic buckling of CSPs for the potential shear walls in high buildings.

Recently, researchers have begun to study the mechanical properties of thin CSPSWs, which buckle in the stage of elastic loading, including ultimate strength, failure modes, and key parameters. Kalali et al., 2015, 2016 investigated the hysteretic performance of CSPSWs. The results indicated that an appropriate design of boundary frame members can yield high stiffness, strength, and cyclic performances of CSPSWs. Berman et al., 2011 compared the performances between a CSPSW and a flat steel plate shear wall (FSPSW), which indicated that the former showed a lower demand for the strength and stiffness of surrounding frames. Emami et al., 2013 investigated the behaviour of CSPSWs with thin CSPs, which showed elastic buckling in the early elastic loading stages and a tension field action failure mode. Shon et al., 2017 conducted an experimental study to investigate the effects of CSP placement on the buckling modes of CSPSWs. The results showed that the failure mechanism varied according to the arrangement of CSPs in the surrounding frames. The CSPSW specimen with a vertical CSP demonstrated a local buckling followed by global buckling, whereas that with a horizontal CSP presented global buckling. Farzampour et al., 2015 proposed an expression to estimate the ultimate capacity of a CSPSW with openings by linear regression analysis.

Researchers have investigated the buckling strength of thin CSPSWs. Dou et al., 2016, 2018 examined the elastic shear buckling and post-buckling strength of sinusoidally CSPSWs by FEA and established fitting equations for the elastic buckling capacity and post-buckling of the shear walls. Wei et al., 2015 studied the elastic shear buckling strength of CSPSWs with edge stiffeners by FEA. The results showed that the local buckling of the corner could
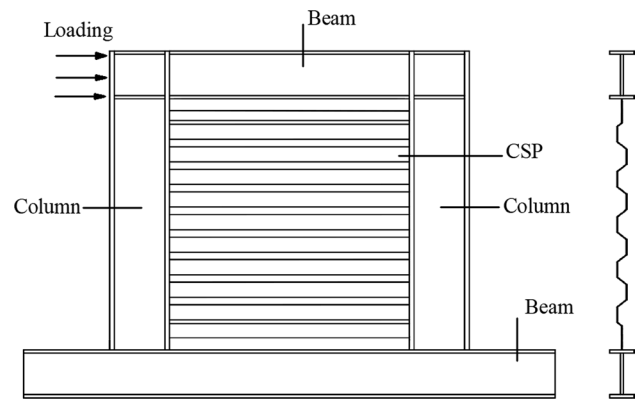
affect the capacity of the shear walls. Farzampour et al., 2015 derived the elastic buckling and ultimate capacity of CSPSWs based on the plate–frame interaction (PFI) method. The result showed that the PFI method could accurately predict the elastic buckling and ultimate capacity of CSPSWs with interactive buckling.

As presented above, previous studies primarily focused on the elastic and-post buckling strengths of thin CSPSWs. However, studies that elaborate the hysteretic performance of CSPSWs with larger thickness corrugated steel plates with inelastic buckling are fewer, of which buckling modes are inelastic buckling. This paper addresses the seismic behaviour of the CSPSWs with inelastic buckling under lateral loads. A numerical model was developed to simulate the performance of CSPSWs with inelastic buckling of CSPs. Buckling modes, post buckling, failure modes of the shear walls were discussed. Bedsides these, the effects of geometric parameters on the seismic behaviour of CSPSWs subjected to lateral loads are investigated as well, such as, height–thickness ratio, aspect ratio, horizontal panel width, corrugation angle, initial imperfections. And the minimum stiffness of the CSPSWs are also discussed. In addition, the ductility, energy dissipation lateral deformation capacity and weak parts of the CSPSW are evaluated to evaluate the seismic performance of the CSPSW with inelastic buckling of the CSP.

2 Computational Study

2.1 Finite Element Model

A single-bay, one-storey CSPSW specimen with a corrugated steel plate horizontally arranged is designed. The specimen size and loading conditions are shown in Fig. 2. In the shear wall structure, the connections between columns and top and bottom beams are rigid. The out-of-plane

deformations of the frames are constrained by lateral braces. The base of bottom beam was fixed.

A numerical model is developed to simulate the seismic performance of a CSPSW using finite element (FE) software ANSYS. A four-node element (shell 181) with six degrees of freedom at each node, which supports full and reduced integration schemes, is adapted to simulate the nonlinear behaviour of CSPSWs. The bilinear kinematic and ideal inelastic model of materials of frames and CSPs are adopted in Fig. 3. The steel elastic modulus of the frames and the CSPs are 2.06×10^{11} N/m^2. The yield strength of CSPs are 370.2 Ma. The yield strength of the frames are 400 Ma, and the ultimate strength of frames are 570 Mpa.

For the bottom boundary conditions of the CSPSWs are fixed. The out-of-plane initial imperfection value of the CSP is set as one thousandth of the width of the CSPs, which is taken into consideration for the manufacturing and installation errors of the CSPs. When the element sizes of models are 20 mm × 20 mm, the results of FE models are insensitive to the element size. The meshed finite element model is shown in Fig. 4.

2.2 Verification Study

The rationality and accuracy of the FE model is verified by a well-known test. A single-bay, two-storey CSPSW specimen test was conducted by (Li & Qiuhong, 2016), of which buckling mode is inelastic buckling modes of CSPs.

In the specimen, the sections of the columns are H-200 mm × 200 mm × 8 mm × 12 mm, and of the top beams H-175 mm × 175 mm × 8 mm × 10 mm, and of the middle beams H-175 mm × 175 mm × 8 mm × 10 mm respectively. The thicknesses of the CSPs are 2 mm. The wave length of the CSPs are 200 mm, the corrugation depth of the horizontal panels 20 mm, and horizontal panel width 50 mm.
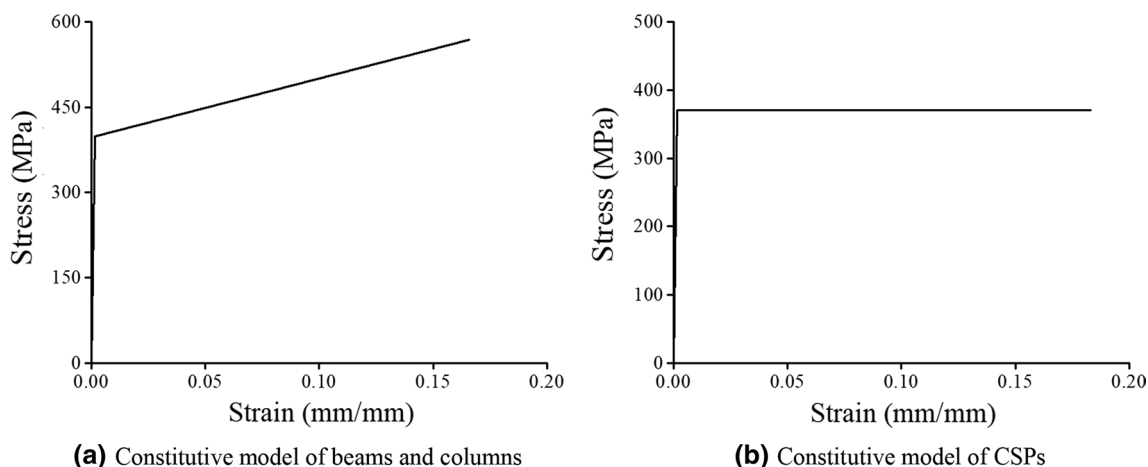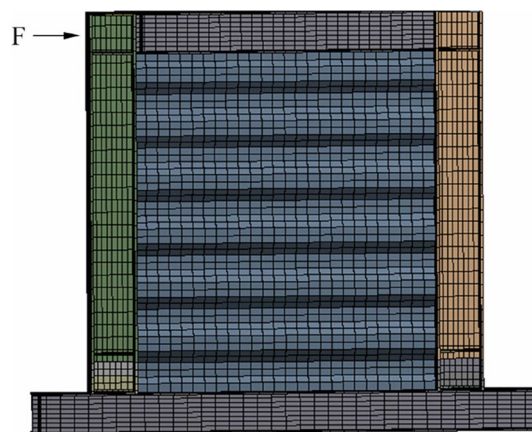

Fig. 4 Meshed finite element model

The comparison of load—displacement curves and failure modes under cyclic loading between the FE model and the CSPSW specimen are carried out in Figs. 5 and 6.

Figure 5 shows the comparison of hysteresis curves between the FE model and the test. The maximum relative errors in the ultimate capacity and the corresponding lateral displacement to ultimate capacity of between the FE model and the test are 7.0% and 13.9%, and the response of the FE model are higher than those of the test. The results of the former and the latter are in good agreement. According to (Li & Qiuhong, 2016), the failure modes of the shear wall is tear failure of bottom the CSP owing to the tension field, which is along the diagonal of the infilled plate, and the phenomenon is also observed in the FE model in Fig. 6. Therefore, the FE model established in this paper could well simulate the hysteretic behaviour of the CSPSW.
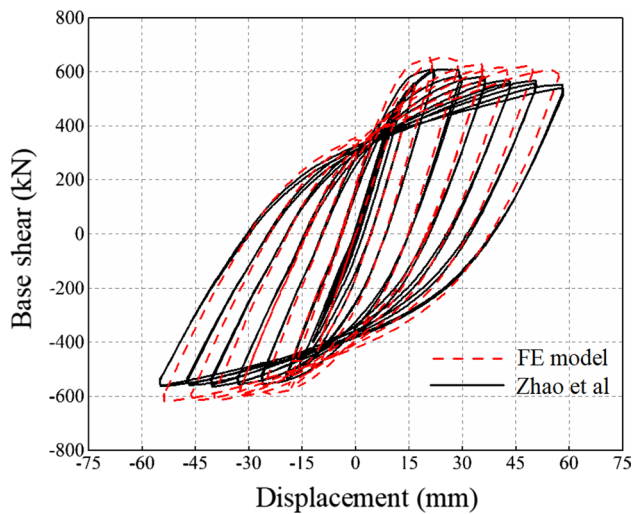

(a) Constitutive model of beams and columns

(b) Constitutive model of CSPs

Fig. 3 Constitutive model of the CSPSW material

Fig. 5 Validation of FE model results
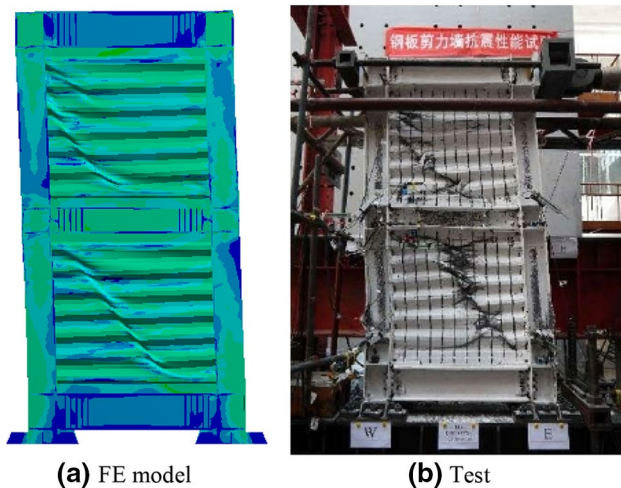

(a) FE model   **(b)** Test

Fig. 6 The verification of failure modes between the FE model and the test results (Li & Qiuhong, 2016)

3 Parametric Analyses and Discussions

In this section, the effects of geometric parameters of the height—thickness ratio, aspect ratio, horizontal panel width, corrugation angle, initial imperfection, and surrounding frame stiffness on CSPSWs are investigated. The details of the parameters study of CSPSWs are shown in Table 1.

3.1 Height—thickness ratio

The height—thickness ratio that is considered to examine the effect on the structure performance of the CSPSW, and five specimens with different height to thickness ratios 100, 200, 300, 500 and 700 are used, with corresponding corrugated plate thickness t_w 10.0 mm, 5.0 mm, 3.3 mm, 2.0 and 1.4 mm respectively. In these models, the sections of the columns are H-250×250×9×14 and of the beams H-200×100×5.5×8 respectively. The geometric characteristics of these CSPs are shown in Table 2. The hysteresis curves with various height—thickness ratios are shown in Fig. 7.

As can be seen in Fig. 7, the shapes of hysteresis curves are spindle. With the decrease of the height—thickness ratio, the shape of the hysteresis curves of the wall is much fuller. When the height—thickness ratio is 700, obvious pinching is observed. The ultimate shear stress is 170.2 MPa, of which ultimate shear stress is less than 0.80 τ_y, and the buckling mode of the CSP is elastic buckling. However, when the height—thickness ratio λ is less than 500, there are no obvious strength and stiffness degradations in these specimens. The buckling mode of the CSPs are inelastic buckling of CSPs ($\lambda \leq 500$), and the shapes of the CSPSWs are different from those of the FPSWs and the thin CSPSWs (Emami et al., 2013; Zhang et al., 2018). The height—thickness ratios of corrugated steel sheet in CSPSW specimens (Emami et al., 2013) vary from 0.752 to 1.78 mm, and the corresponding height—thickness ratios λ vary from 700 to 1700. The ultimate shear stress of these CSPSWs in the tests are form 30–35 Mpa, which are much lower than the yield stress of the infilled plates, and the specimens show obvious pinching and degradations in hysteretic curves, of which failure modes are elastic buckling. Therefore, the shapes of the hysteretic curves are much thinner than those of CSPSWs with height—thickness ratios λ from 100 to 500 in this paper. With the increase of height—thickness ratio of a CSP, the shear stress of infilled plates decreases (Fig. 8).

The similar phenomena are also observed in the tests conducted by Massood (Emami et al., 2013), and the height—thickness ratios of CSPSW specimens λ are 1600. In the reference (Emami et al., 2013), the ultimate shear stresses of the CSPs are approximately 100 Mpa, and the corresponding drift ratios are approximately 0.06. It is indicated that drift ratios corresponding to the ultimate strength of the specimens in the tests are much larger than those of the CSPSWs with inelastic buckling of CSPs. This is largely due to larger

Table 1 Key parameters table

Specimens	CSP						Column	Beam
	t_w(mm)	H(mm)	B(mm)	h_r(mm)	b(mm)	θ(mm)	(mm)	(mm)
CW-1	1.4	1046	1000	60	70	60.0°	250×250×9×14	200×200×5.5×8
CW-2	2.0	1046	1000	60	70	60.0°	250×250×9×14	200×200×5.5×8
CW-3	3.0	1046	1000	60	70	60.0°	250×250×9×14	200×200×5.5×8
CW-4	5.0	1046	1000	60	70	60.0°	250×250×9×14	200×200×5.5×8
CW-5	10.0	1046	1000	60	70	60.0°	250×250×9×14	200×200×5.5×8
CW-6	3.3	1046	1500	60	70	60.0°	300×300×30×30	300×300×30×30
CW-7	3.3	1046	2000	60	70	60.0°	300×300×30×30	300×300×30×30
CW-8	3.3	1046	2500	60	70	60.0°	300×300×30×30	300×300×30×30
CW-9	3.3	1046	3000	60	70	60.0°	300×300×30×30	300×300×30×30
CW-10	3.3	1046	1000	25	30	60.0°	250×250×9×14	200×200×5.5×8
CW-11	3.3	1046	1000	43	50	60.0°	250×250×9×14	200×200×5.5×8
CW-12	3.3	1046	1000	77	90	60.0°	250×250×9×14	200×200×5.5×8
CW-13	3.3	1046	1000	95	110	60.0°	250×250×9×14	200×200×5.5×8
CW-14	3.3	1046	1000	35	70	30.0°	250×250×9×14	200×200×5.5×8
CW-15	3.3	1046	1000	42	70	37.5°	250×250×9×14	200×200×5.5×8
CW-16	3.3	1046	1000	49	70	45.0°	250×250×9×14	200×200×5.5×8
CW-17	3.3	1046	1000	55	70	52.5°	250×250×9×14	200×200×5.5×8
CW-18	3.3	1046	1000	60	70	60.0°	125×125×13×7	125×125×13×7
CW-18	3.3	1046	1000	60	70	60.0°	150×150×15×9	150×150×15×9
CW-19	3.3	1046	1000	60	70	60.0°	175×175×13×7	175×175×13×7
CW-20	3.3	1046	1000	60	70	60.0°	190×190×14×8	190×190×14×8
CW-21	3.3	1046	1000	60	70	60.0°	230×230×15×10	230×230×15×10
CW-22	3.3	1046	1000	60	70	60.0°	330×330×15×12	330×330×15×12

Table 2 Geometric characteristics of CSPSWs

t_w(mm)	λ	H(mm)	B(mm)	B/H	d(mm)	h_r(mm)
1.4, 2.0, 3.3,5.0, 10.0	500, 300, 200, 100	1046	1000	1.0	35	60

compression capacity of tension field of the CSPSWs than those of the FPSWs and thin CSPSWs. The larger the height to thickness ratio is, the fuller shape of the hysteresis curves of the CSPSW is.

Figure 9 shows the typical buckling modes of the CSPSW with inelastic buckling of the CSP (λ=300). From Fig. 9, the typical buckling mode of the CSPSW is the inelastic buckling along the diagonals of the CSP. And this is different from that of the CSPSW with small thickness of a CSP and a FPSW (Emami et al., 2013; Zhang et al., 2018), of which buckling mode is elastic buckling shown in Table 3.

The failure modes of CSPSWs are associated with height—thickness ratios. When the height—thickness ratios of the CSPs are 300—700, the failure modes are failure of

tension field formed in the CSPs, of which buckling modes are inelastic buckling, and the way of resisting the lateral loads are tension field shown in Fig. 10b, c. The failure modes of the CSPSWs are consistent with those of the CSPSW specimens with CSP elastic buckling conducted by (Emami et al., 2013). Compared with the CSPSW (λ= 300), the tension field developed more fully shown in Fig. 10c. However, when the height—thickness ratio of the CSPs is less than 200, of which buckling modes is yielding of the CSP, and the way of resisting the lateral loads is pure shear shown in Fig. 10a.

Figures 11 and 12 show the typical trajectory of principal stress and out-of-plane deformation of the CSPs under the failure modes respectively. It is can be seen that the failure
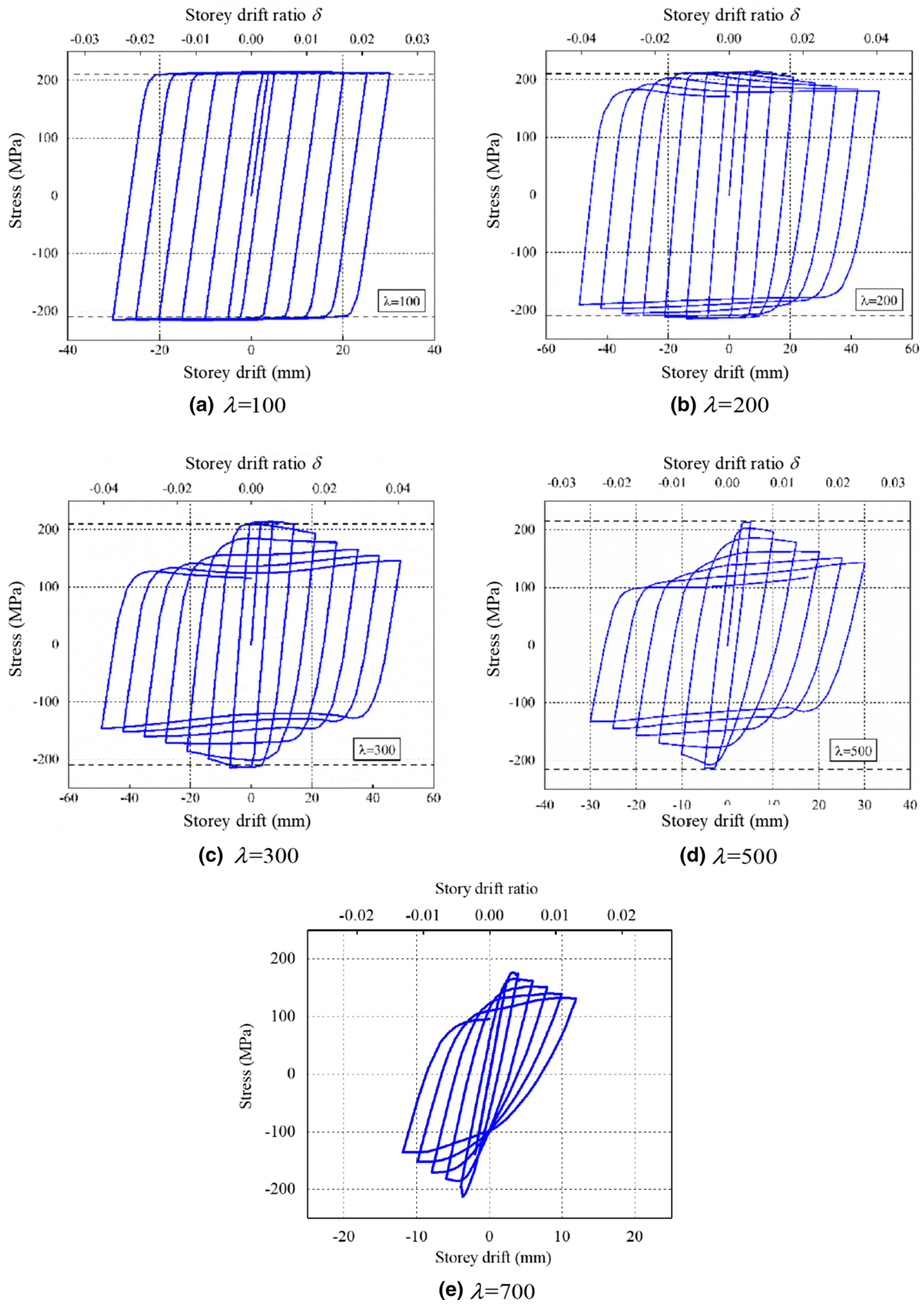
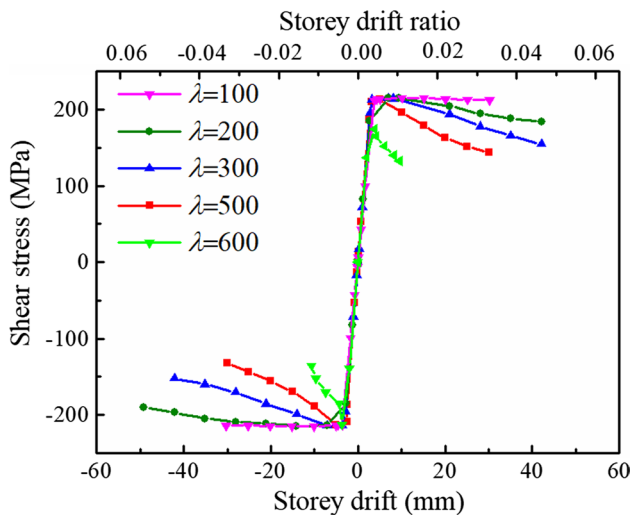**Fig. 7** Hysteresis curves of CSPSWs with different height—thickness ratios

Fig. 8 Skeleton curves with various height to thickness ratios
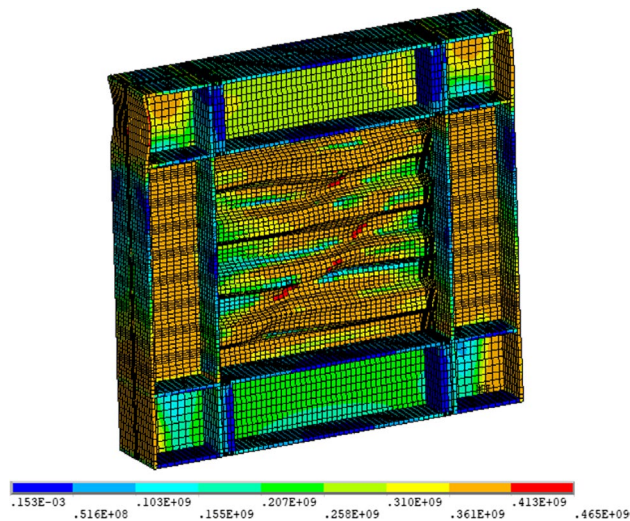

Fig. 9 Inelastic buckling of the CSP (λ=300)

modes of the CSPSW are yielding of the tension field strips along the diagonals in the whole CSP, of which inclination angle of the tension field strips is about 45°. And the corners

in the CSP are the earliest parts to enter the yield stage. So, the corners of the CSPs in shear walls should be strengthened. In practical projects, the corners of infilled plates are usually to be strengthen by reinforcing plates to prevent the stress concentrating. Besides this, the other effective method is cutting the corners of infilled plates in some FSPSWs (Fig. 13).

Skeleton curves and hysteretic energy dissipation curves with height—thickness ratios are shown in Figs. 8 and 14 respectively. The lateral deformation capacity of shear walls is an important index of the ductility of shear walls. After the ultimate strength, the load decrease to the 85 percent of the ultimate strength of the CSPs, the lateral ultimate deformation Δ_u are 60.5 mm, 42.13 mm, 28.08 mm, 15.04, and 8.24 mm respectively, with the corresponding height-thickness ratios 100, 200, 300, 500 and 700 respectively. The lateral ultimate deformation Δ_u shows a negative correlation with the height-thickness ratio. It is because that the lateral shear stiffness of the shear walls is more largely weaken when the CSPs with larger height—thickness ratios buckle. Similar as shown in Fig. 8, the shear walls experience earlier and sharper decrease in strength resistance with the increase of height—thickness ratios.

The ductility coefficient μ could be used to describe the lateral plastic deformation capacity, which are expressed as:

$$\mu = \frac{\Delta_u}{\Delta_y} \tag{1}$$

where Δ_y represents the yield deformation of CSPSWs, Δ_u ultimate displacement.

The ductility coefficient μ of the CSPSWs are 16.1, 12.5, 9.0, 4.9 and 3.0 respectively, when the heigh to thickness ratios are 100, 200, 300, 500 and 700 respectively. When the height—thickness ratios are less than 500, the ultimate lateral deformation Δ_u exceed 0.02. This means that this kind of shear walls show good lateral plastic deformation capacity with appropriate height-thickness ratios.

Besides these, the lateral deformation capacity is very import to the energy dissipation of shear walls. Energy

Table 3 Results of CSPSWs with different—thickness ratios	Height-thickness ratio	Yield displacement Δ_y	Yield strength τ_y	Ultimate displacement Δ_u	Ultimate strength τ_u	Ductility coefficient μ
	λ	(mm)	(MPa)	(mm)		
	100	3.76	212.2	60.50	215.1	16.1
	200	3.36	211.3	42.13	214.6	12.5
	300	3.13	211.2	28.08	214.5	9.0
	500	3.07	209.2	15.04	213.6	4.9
	700	2.72	170.2	8.24	177.0	3.0

(a) λ=200

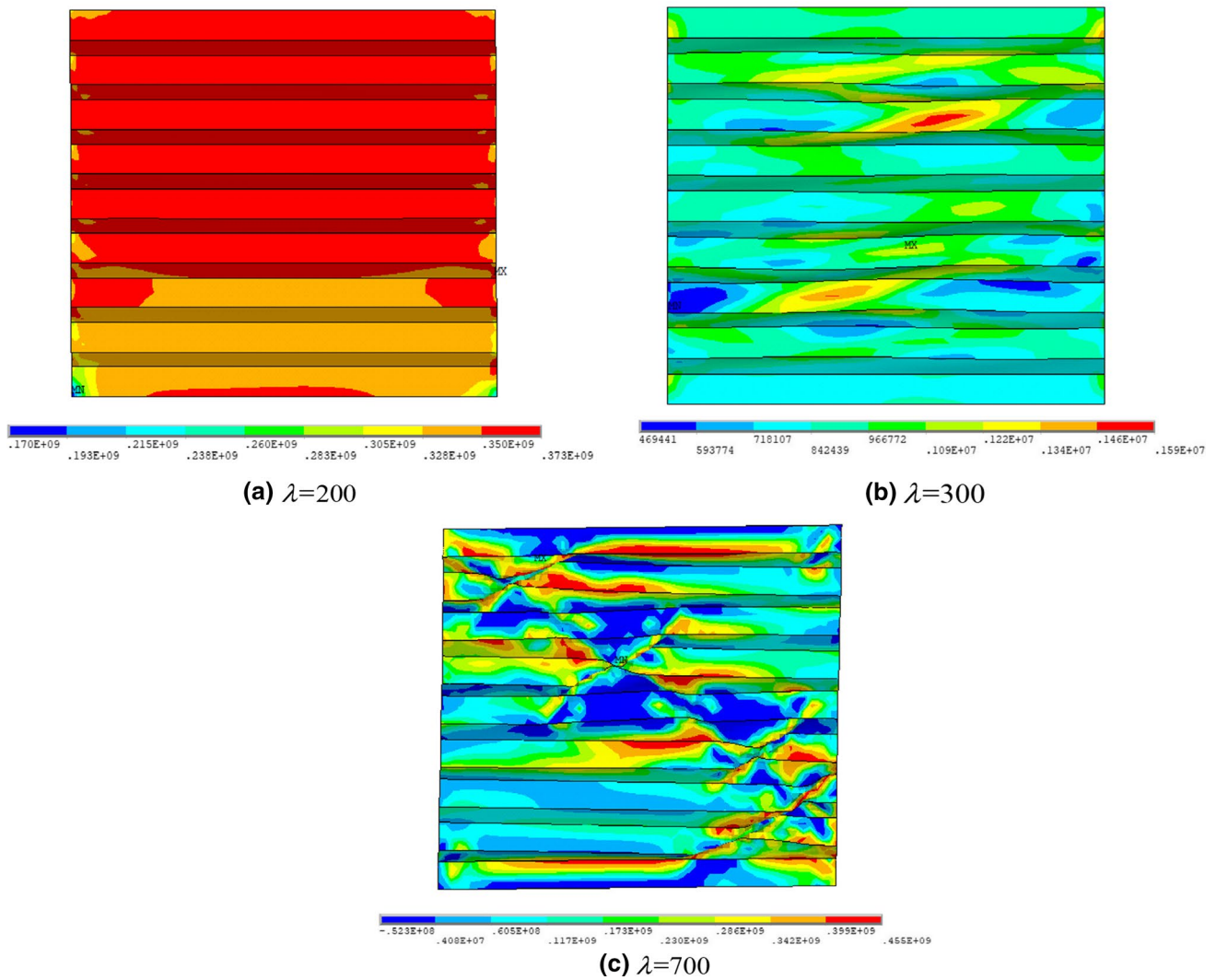**(b)** λ=300

(c) λ=700

Fig. 10 Failure modes of CSPs with different ratios

dissipation coefficient E_n could be used to evaluate the dissipation capacity, and the index E_e could be expressed as:

$$E_n = \frac{S_{ABCDA}}{S_{OBE} + S_{OAF}} \tag{2}$$

S_{ABCDA} represent the area enclosed by hysteresis curve in Fig. 13, $S_{OBE} + S_{OAF}$ represent the areas of the triangles OBE and OAF in Fig. 13.

The energy dissipation coefficient curves are shown in Fig. 14. The figure shows that the coefficient E_n decreases with the increase of the height—thickness ratio. This is because the thickness of the infilled CSPs could significantly improve the energy consumption capacity of the shear walls.

3.2 Aspect Ratio

In this part, four specimens with different aspect ratios, 1.5, 2.0, 2.5, and 3.0 were used to study the effect of aspect ratios on cyclic performance of the CSPSW. In these models, aspect ratios were adjusted by changing the CSPs width B,
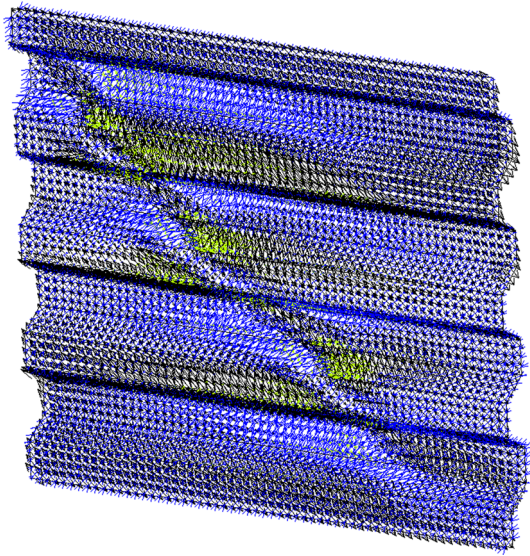
Fig. 11 Typical trajectory of principal stress of the CSP under the failure mode (λ=300)
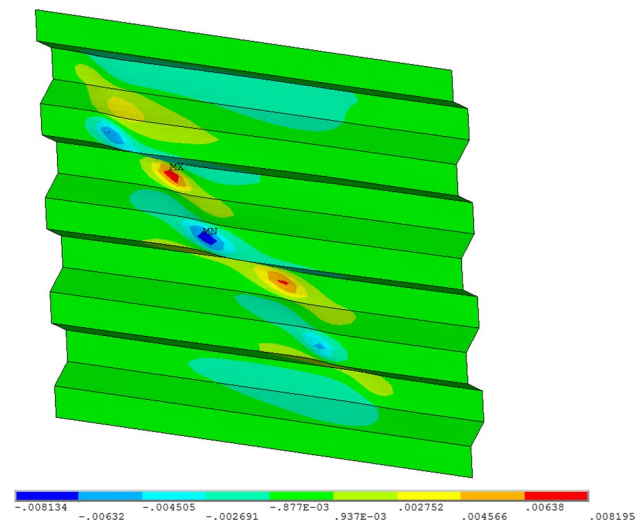
Fig. 12 Out-of-plane deformation of the CSP under the failure mode (λ=300)

with height of these models H unchanged. The geometric characteristics of these CSPs are shown in Table 4.

Figure 15 shows that the shapes of hysteresis curves become much thinner with the increase of aspect ratios, and when the aspect ratios reach to 2.0, and the pinching phenomena become obvious. Buckling capacity and ultimate
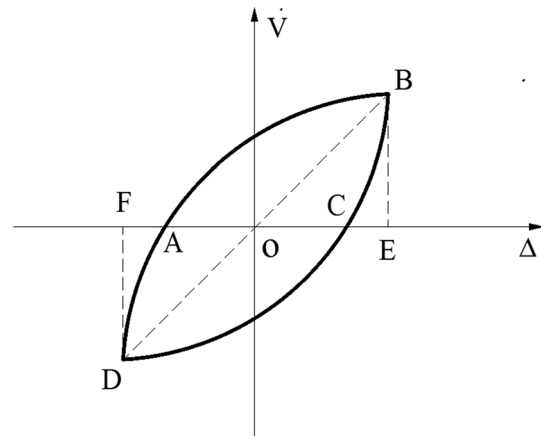
Fig. 13 Calculation of energy dissipation coefficient
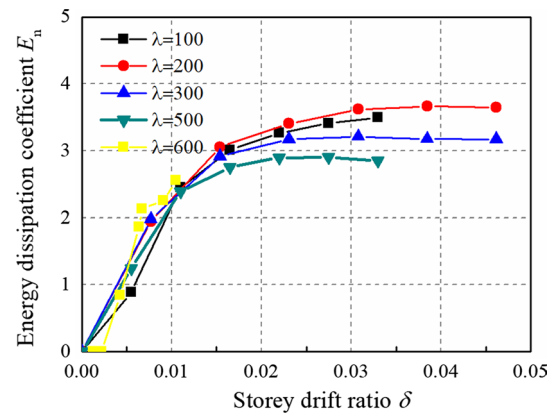
Fig. 14 Energy dissipation coefficient curves with different height—thickness ratios

capacity of CSPs decrease with the increase of aspect ratios. This is because the buckling capacity decrease with the increase of the aspect ratio.

The skeleton curves of the hysteresis curves with aspect ratios are shown in Fig. 16. As can be seen from the figure, the ultimate strength of the CSPs decreases with the increase of the aspect ratio B/H As the CSP width of increases, the constrains of surrounding frames on CSPs become weaker, so the average value of ultimate stress in the transverse section of the CSPs reduces. The energy dissipation coefficient shows a reverse trend with the increase of the aspect ratio in Fig. 17.

Table 4 Geometric characteristics of CSPSWs

B(mm)	B/H	H(mm)	λ	d(mm)	h_r(mm)	b(mm)
1500, 2000, 2500, 3000	1.5, 2.0, 2.5, 3.0	1000	300	35	60	70

(a) $B/H = 1.5$

(b) $B/H = 2.0$
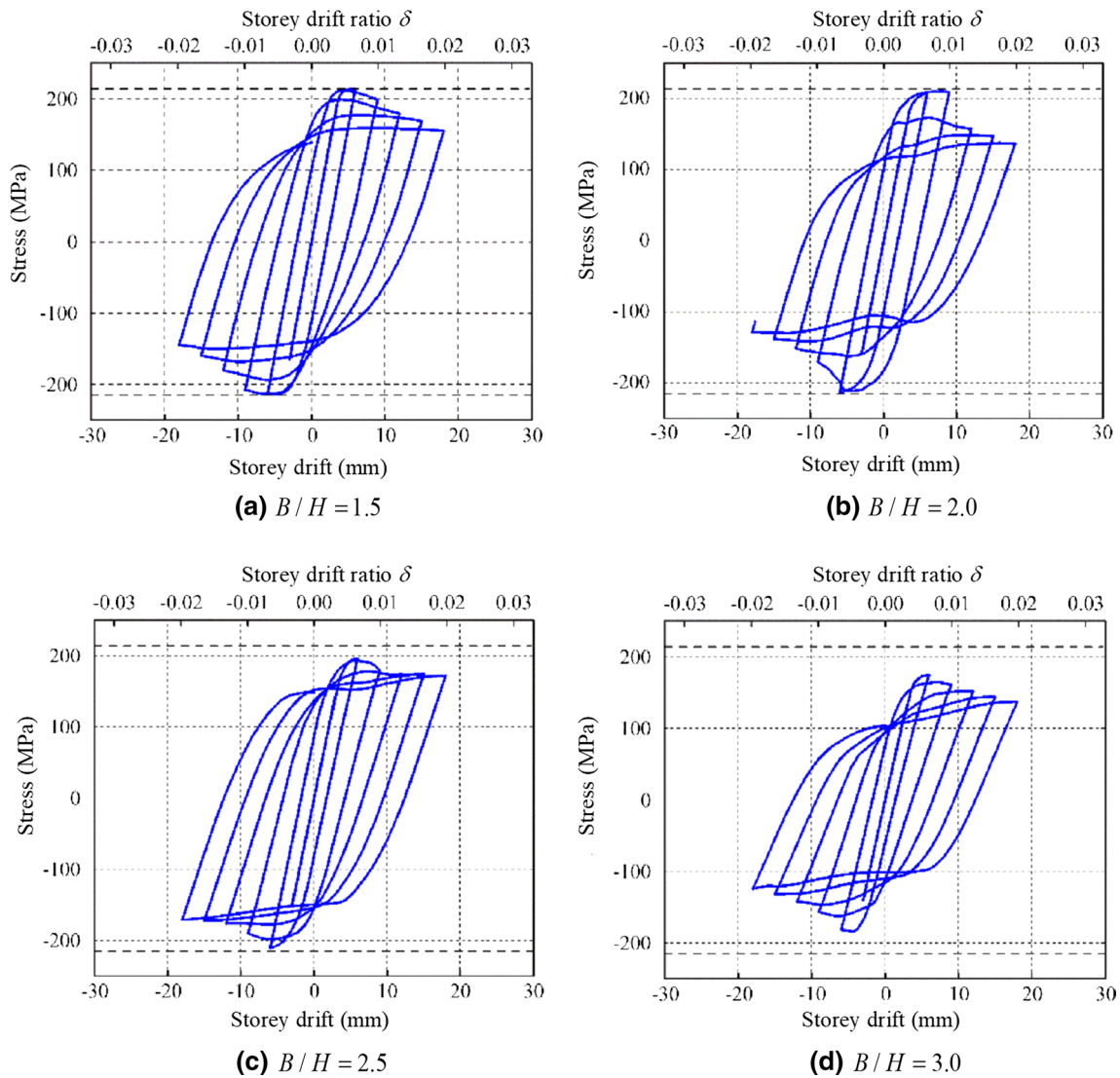
(c) $B/H = 2.5$

(d) $B/H = 3.0$

Fig. 15 Hysteresis curves of CSPSWs with different aspect ratios

3.3 Horizontal Panel Width

To study the effect of the horizontal panel width on the performance of the CSPSW, four specimens with different horizontal panel widths of 30 mm, 50 mm, 70 mm, 90 mm, and 110 mm were used. The geometric characteristics of these CSPSWs are shown in Table 5.

Figure 18 shows that with the increase of horizontal panel width, the shapes of hysteresis curves become much fuller and there are no obvious pinching phenomenon in the these curves. And the strength capacity drops slowly after the ultimate with the increase of the horizontal panel width. The skeleton curves and the hysteresis curves with horizontal
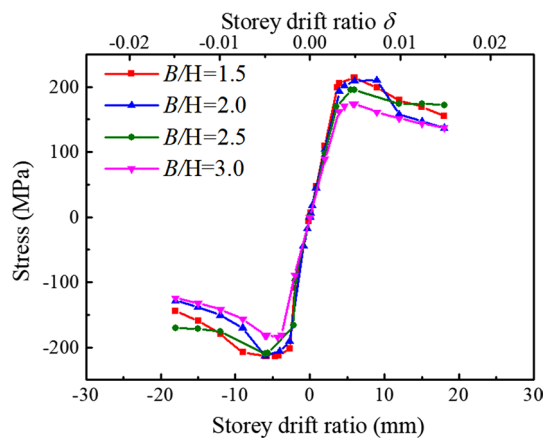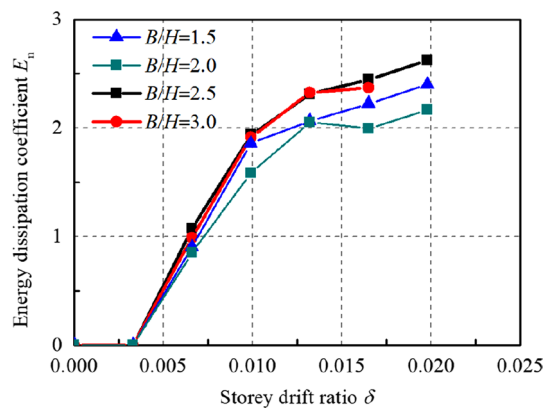
Fig. 16 Skeleton curves with different aspect ratios

Fig. 17 Energy dissipation coefficient curves with different aspect ratios

Table 5 Geometric characteristics of CSPSWs

b(mm)	λ	H (mm)	B (mm)	d (mm)	h_r (mm)
30, 50, 70, 110	300	1000	1000	35	60

panel width are shown in Figs. 19 and 20 respectively. The skeleton curves and hysteresis curves are independent of the horizontal panel width.

3.4 Corrugation Angle

To study the effect of corrugation angles on the behaviour of the CSPSW, four specimens with different corrugation angles θ of 30°, 37.5°, 45°, and 52.5° were used. The geometric characteristics of these CSPSWs models are shown in Table 6.

Figures 21 and 22 show hysteresis curves and skeleton curves of CSPSWs with different corrugation angles of the CSPs. From Fig. 21 and 22, after the ultimate strength, a smaller corrugation angle results in a faster decline in the bearing capacity of the CSP. That's because when a smaller corrugation angle means a smaller moment of inertia. It can be concluded that the energy absorption capability has a positive relationship with the corrugation angle from Fig. 23.

3.5 Initial Imperfection

To study the effect of initial imperfection on the performance of the CSPSW, four specimens with different initial imperfections of $\lambda/10000$, $\lambda/100$, $\lambda/50$, and $\lambda/20$ were used. The geometric characteristics of these CSPSWs are shown in Table 7. Figure 24 shows hysteresis curves of CSPSWs with different initial imperfections.

The hysteretic behaviour of the CSPs is insensitive to the initial imperfection shown in Figs. 24 and 25. This is because the initial imperfections have little effect on the buckling and ultimate capacity of the CSPs owing to its own corrugations of CSPs.

3.6 Surrounding Frame Stiffness

As the boundary conditions of steel plate shear walls, surrounding frames are essential to the loading mechanism and buckling capacity of shear walls. The Design of Steel Structures (CAN/CSA-S16-09) (Association & CAN, CSA-S, 1601, 2001) and Seismic Provision for Structural Steel Buildings (ANSI/SISC 341–05) (Institute & of Steel Construction. ANSI, AISC341–05, 2005) used Montgomer's (James & Manoj, 2001) research results and suggested that the minimum value of inertia moment of columns should satisfy Eq. (3).

$$I_{cmin} \geq 0.00307 t_w d_s^4 / b_s \tag{3}$$

The Eq. (3) is based on the research results of the FSPSW, which is closely related to the compression performance of the infilled steel plates and stiffness of the surrounding frames. However, the CSPs show strong anisotropy in parallel to and perpendicular to waves directions. Besides these, the buckling modes, failure modes, and loading mechanism of the CSPSWs differ from those of FSPSWs. Therefore, the effect of the surrounding frame stiffness on the performance of the CSPSW should be discussed.
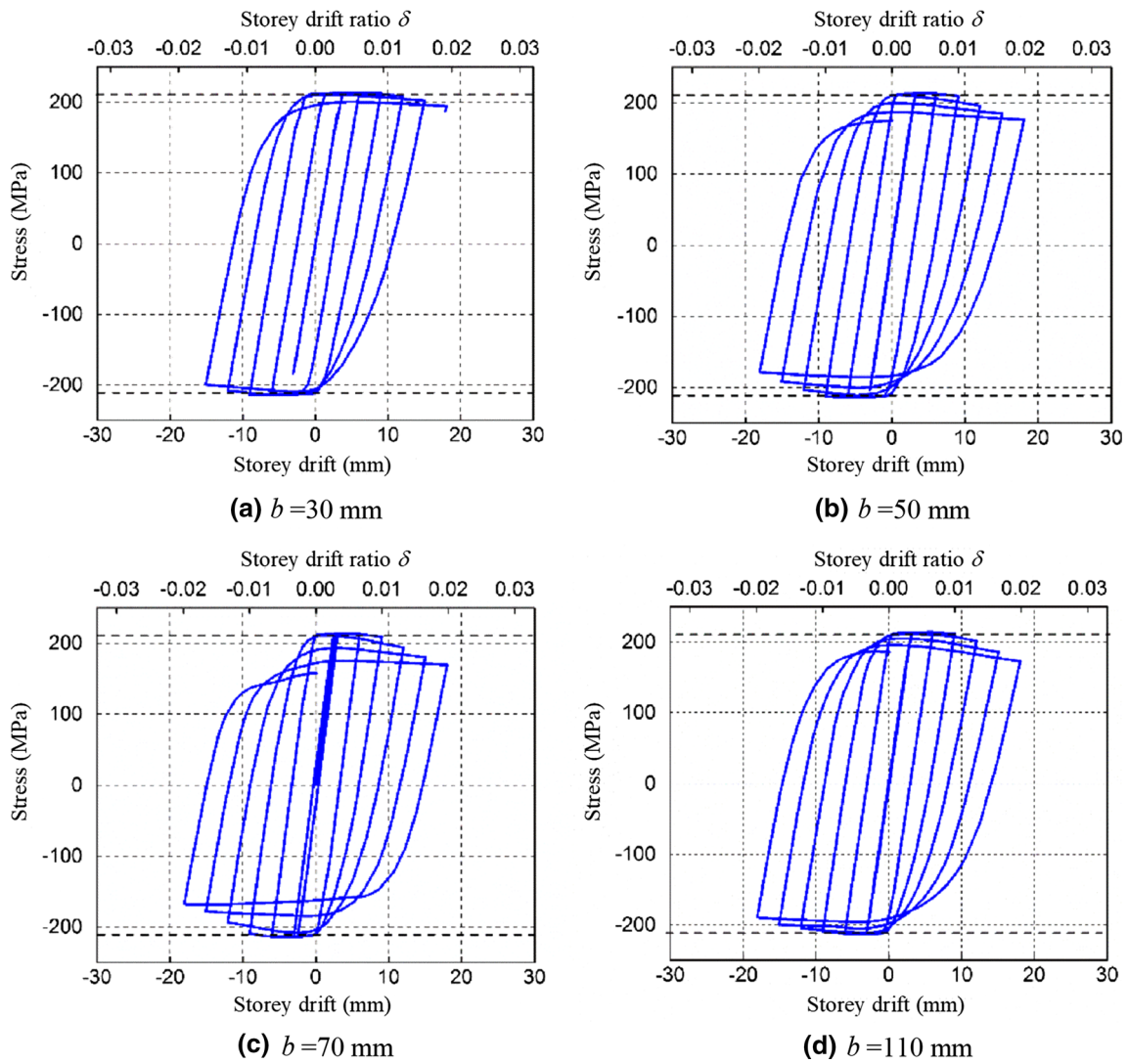
(a) $b = 30$ mm

(b) $b = 50$ mm

(c) $b = 70$ mm

(d) $b = 110$ mm

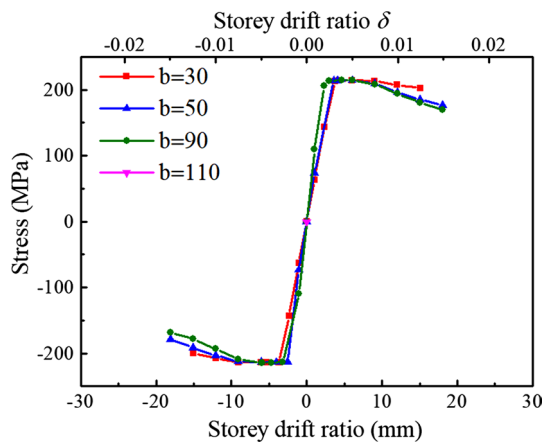**Fig. 18** Hysteresis curves of CSPSWs with different horizontal panel width
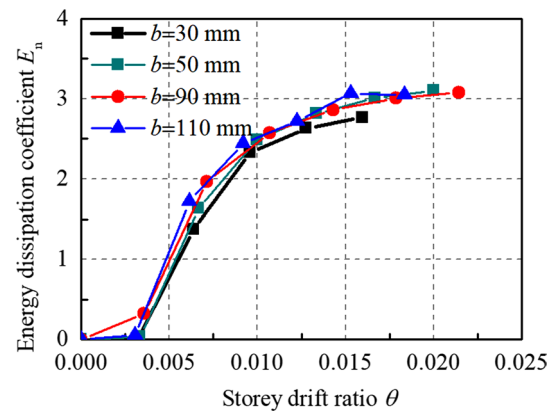

Fig. 19 Skeleton curves with horizontal panel width

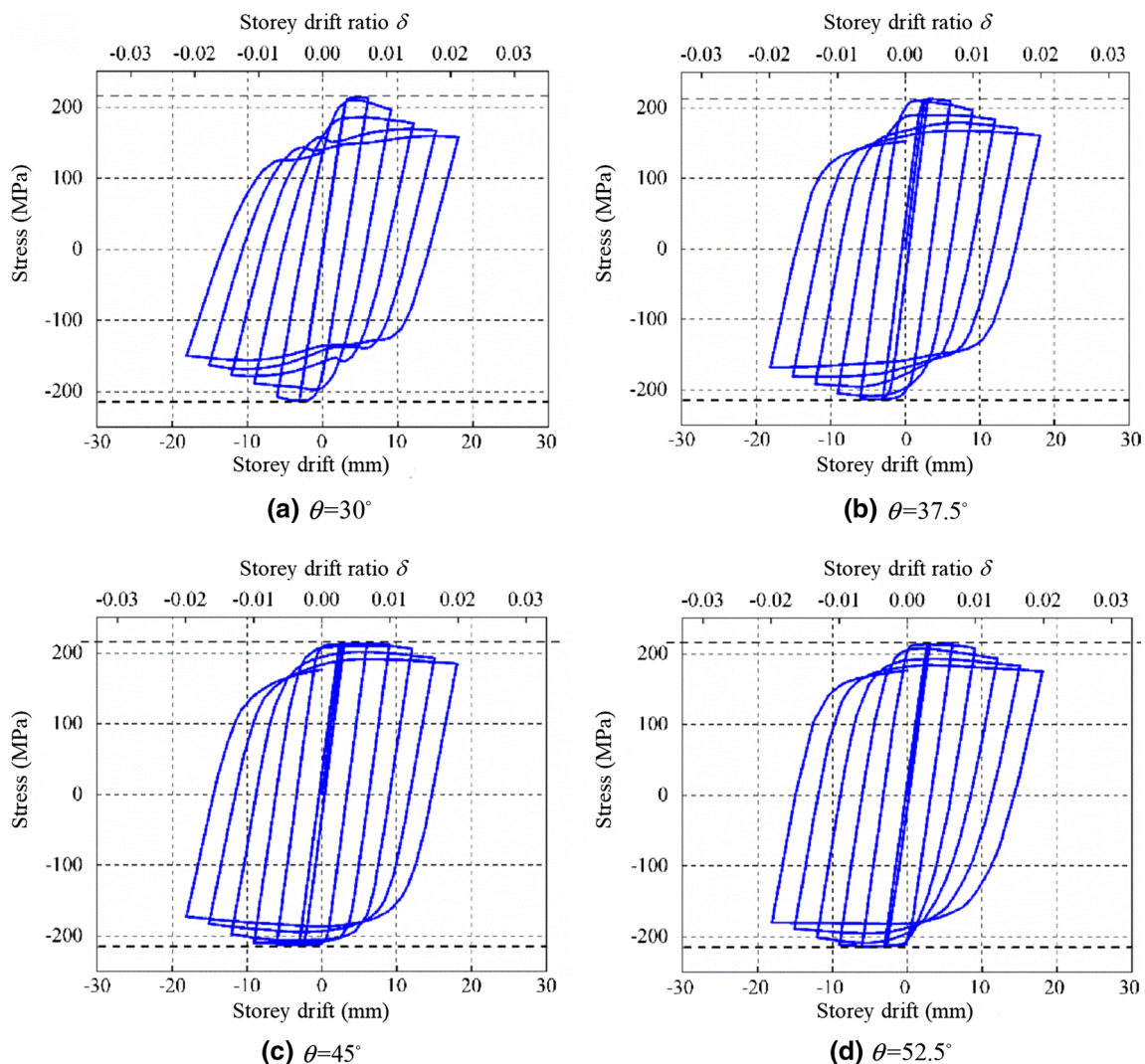**Fig. 20** Energy dissipation coefficient curves with different horizontal panel width

Table 6 Geometric characteristics of CSPSWs

θ	λ	H (mm)	B (mm)	d (mm)	b (mm)
30°, 37.5°, 45°, 52.5°	300	1.046	1000	35	70

In this part, four specimens of CSPSWs ($\lambda = 300$) were used for study the effect of surrounding frame stiffness on the hysteretic performance of the CSPSW, with 0.5 $I_{c\min}$, $I_{c\min}$, 2 $I_{c\min}$, and 10 $I_{c\min}$ respectively. In these models, the corresponding sections of the columns were $HW125 \times 125 \times 13 \times 7$, $HW150 \times 150 \times 15 \times 9$, $HW175 \times 175 \times 13 \times 7$, $HW190 \times 190 \times 14 \times 8$, $HW210 \times 210 \times 15 \times 9$, $HW230 \times 230 \times 15 \times 10$, and $HW330 \times 330 \times 15 \times 12$ respectively. The load—displacement curves with various columns stiffness are shown in Fig. 26.

When the surrounding frame stiffness $I_c = 0.5I_{c\min}$, there are obvious pinching phenomenon in the load—displacement curves. With the increase of the surrounding frame stiffness, the shapes of the hysteresis curves of the wall are much fuller. When the surrounding frame stiffness reach $I_{c\min}$, the pinching phenomenon disappears. This is because that when column stiffness $I_c < I_{c\min}$, the stress of tension field is not uniformly, which decrease from the center tension field strips to the neighbouring tension field strips. However, when the columns stiffness is greater than $I_{c\min}$, the stress of tension field plate of the CSP distribute uniformly, and most of tension field strips yield (Fig. 27).

Besides these, bearing capacity and energy dissipation capacity have a positive with the increase of the surrounding frame stiffness. This means that surrounding columns with $I_c \geq I_{c\min}$, could provide sufficient supports for the full development of tension fields.

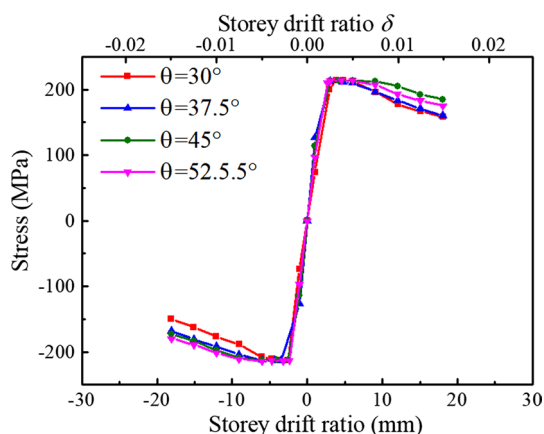**Fig. 21** Hysteresis curves of CSPSWs with different corrugation angles

Fig. 22 Skeleton curves with different corrugation angles
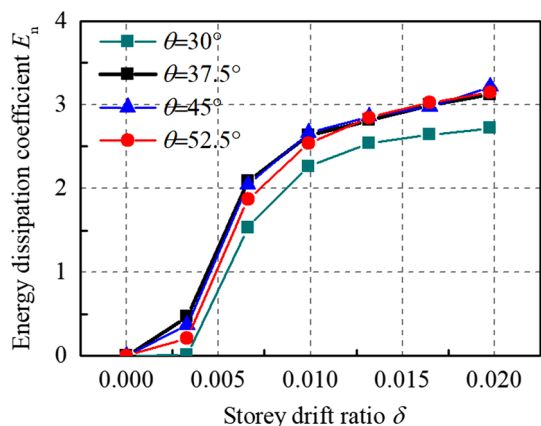

Fig. 23 Energy dissipation coefficient curves with different corrugation angles

Besides these, the surrounding frames stiffness also plays important in the buckling capacity of the CSPs. As shown in Fig. 28, the buckling capacity of the CSPs increases with increase of the surrounding frame stiffness I_c. When the stiffness of the frame I_c is greater than $I_{c\,min}$, the buckling strength of the CSPs tends to be stable. This is primarily because the increase in stiffness of the surrounding columns

could more effectively restrict the out-of-plane deformation of the CSPs, resulting in the increase of buckling strength of the CSPs.

It is noticeable that the stiffness of surrounding frame sections should satisfy Eq. (3). Subsequently, the buckling strength and energy dissipation capacity of the CSPSWs tend to be stable, and the surrounding frames provide a sufficient anchoring effect to CSPSWs.

4 Conclusions

The seismic performance of CSPSWs with inelastic buckling of CSPs subjected to lateral loads are investigated in this study. A CSPSW specimen is designed to study the hysterics behaviour of the CSPSWs, and the effects of those key parameters on the hysteretic behaviour of CSPSWs were studied. The main conclusions are as follows:

(1) The buckling modes of the CSPSW with inelastic buckling of CSPs are the inelastic buckling along the diagonals of CSPs, and the way of resisting the lateral loads rely on tension field. After the buckling, the CSPSWs could resisting greater load by the tension field. The corresponding failure mode of the CSPSW is failure of the tension field strips along the along the diagonals in the whole CSP, of which inclination angle of the tension field strips is about 45°.

(2) The corners in the CSP are the earliest parts to enter the yield stage, and the corners are the first lactation to be destroyed in the shear walls under lateral loads. Therefore, the corners of CSPs in CSPSWs should be strengthened in future designs.

(3) The height—thickness ratio has a great effect on the strength of the CSPSWs. When the heigh-thickness ratio exceeds 500, the strength drops significantly after the ultimate strength. This phenomenon also occurs in the CSPSWs with a large aspect ratio. It is suggested that the values of height—thickness ratios and the aspect ratios of the CSPSWs should be restricted in the design of the high buildings. Initial imperfections

Table 7 Geometric characteristics of CSPSWs	Initial imperfections	λ	H (mm)	B (mm)	d (mm)	b (mm)	θ
	$\lambda/10000$, $\lambda/100$, $\lambda/50$, $\lambda/20$	300	1046	1000	35	70	60°

(a) $n\lambda = \lambda/20$

(b) $n\lambda = \lambda/50$

(c) $n\lambda = \lambda/100$
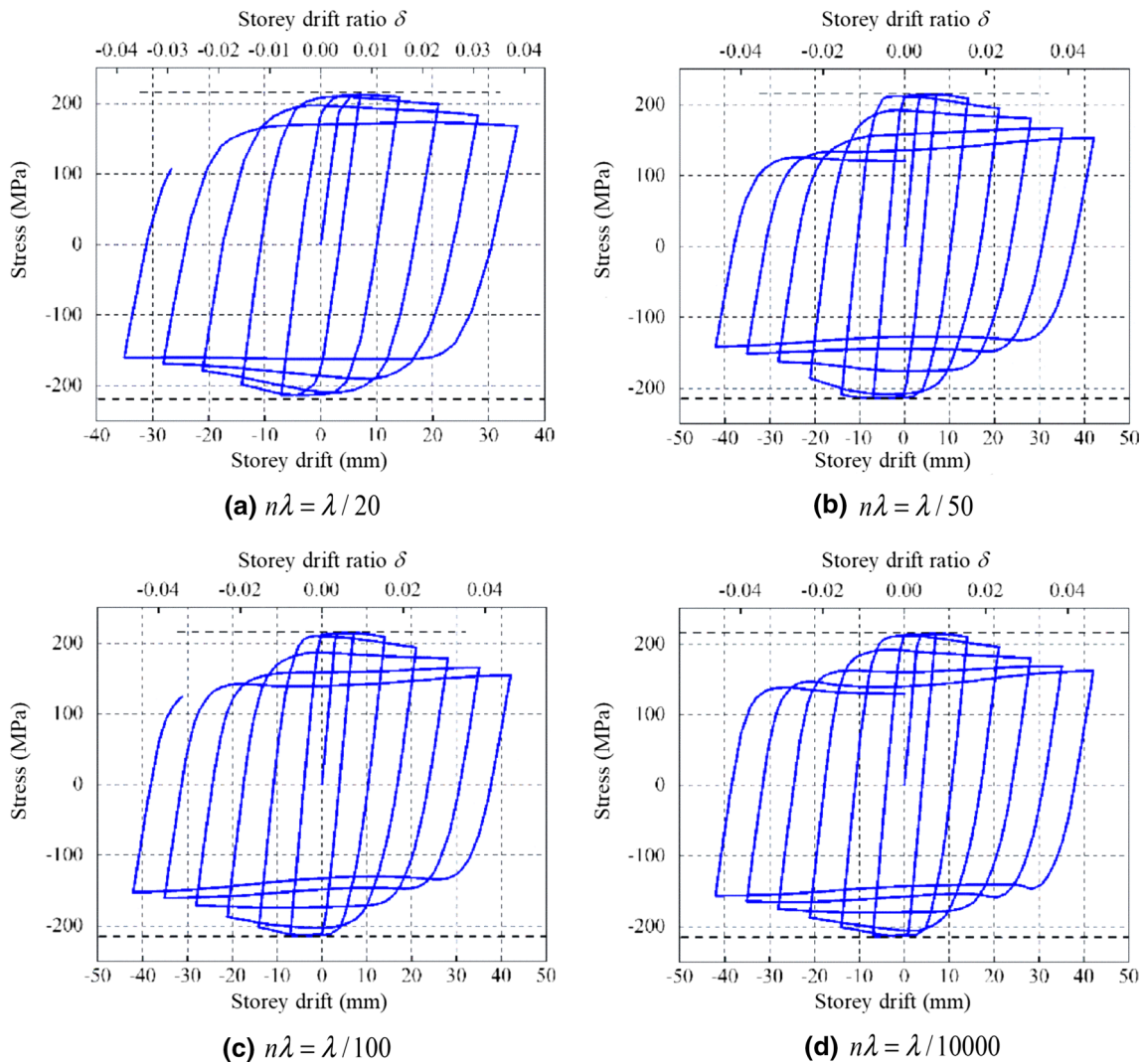
(d) $n\lambda = \lambda/10000$

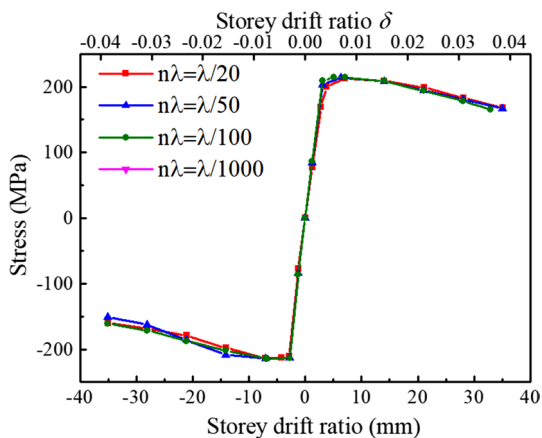**Fig. 24** Hysteresis curves of CSPSWs with different initial imperfections

Fig. 25 Skeleton curves with various initial imperfections

have little effect on the seismic behaviour of the CSPs owing to its own corrugation.

(4) The lateral plastic deformation capacity of the CSPSW decrease with the increase of the height—thickness ratio. And when the height—thickness ratios are less than 500, the ultimate lateral deformation of CSPSW Δ_u exceed 0.02. It is indicated that the CSPSWs show good lateral plastic deformation capacity with appropriate height-thickness ratios.

(5) The surrounding frames stiffness I_c could affected the energy-dissipating capacity and the buckling capacity of the CSPSWs. When the surrounding frame stiffness $I_c \geq I_{c\,\min}$, the energy dissipating capacity and the buckling capacity of the CSPSWs tends to be stable.
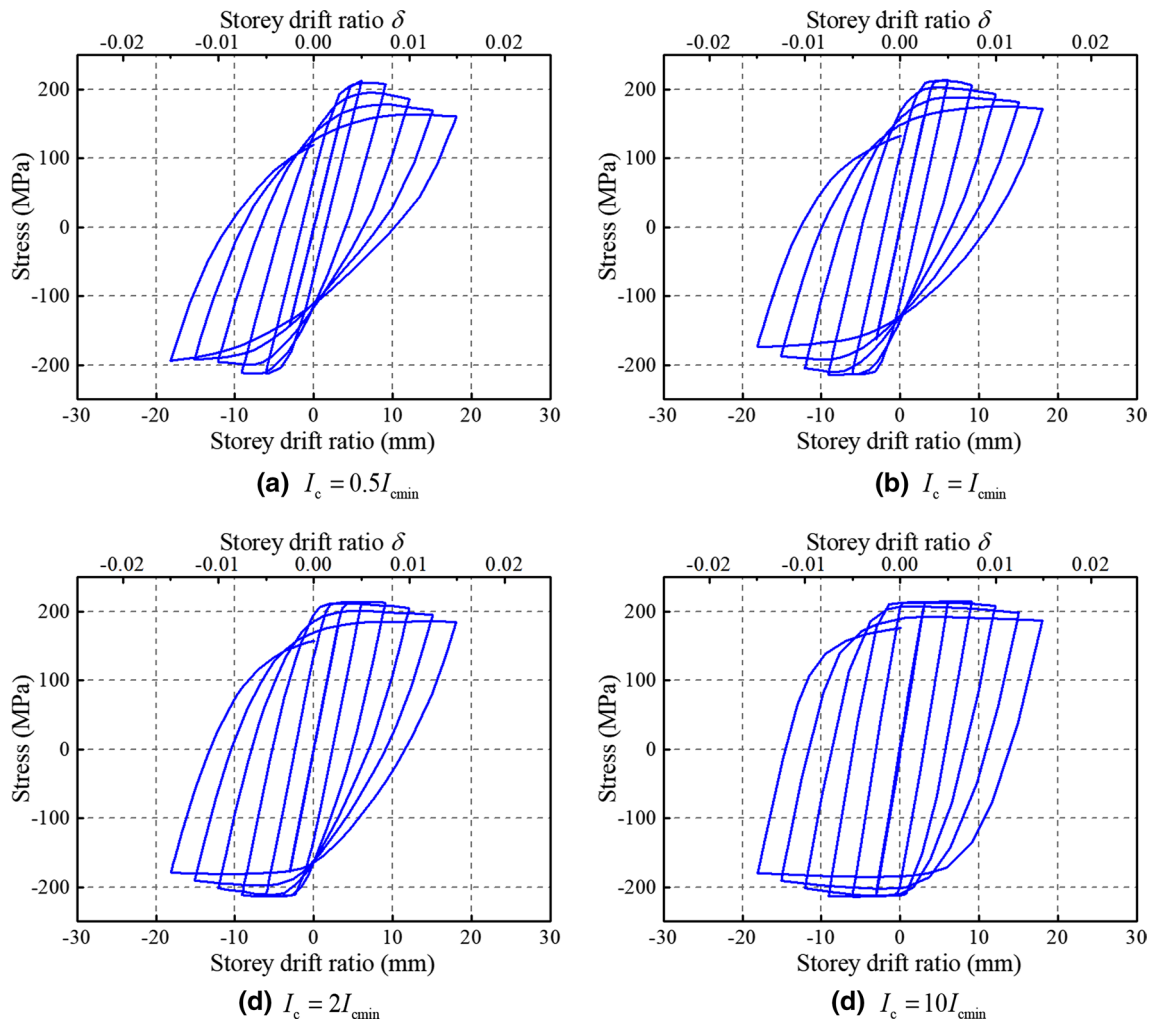
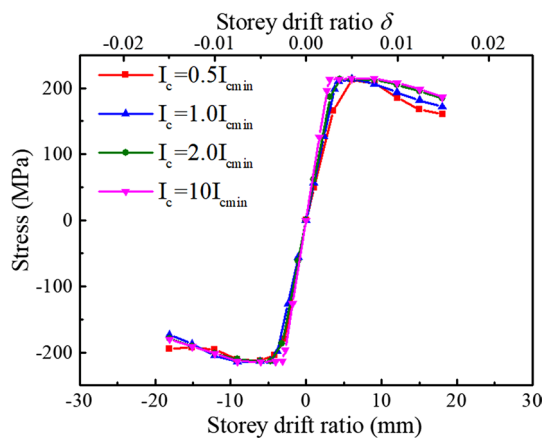**Fig. 26** Load—displacement curves of CSPSWs with various surrounding frame stiffness

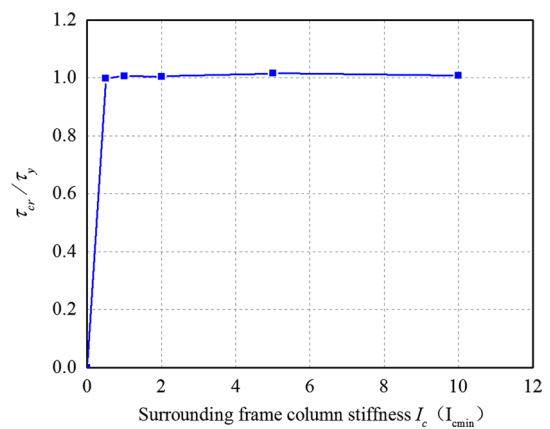**Fig. 27** Skeleton curves with different surrounding frame stiffness

Fig. 28 Buckling capacity versus frame stiffness curve

Data availability Not applicable.

Code availability Not applicable.

Declarations

Conflict of interest The authors declared that they have no conflicts of interest to this work. We declare that we do not have any commercial or associative interest that represents a conflict of interest in connection with the work submitted.

Ethical approval Not applicable.

Consent to participate Not applicable.

Consent for publication Not applicable.

References

American institute of steel construction (2005). ANSI/AISC 341–05. AISC committee. Seismic provision for structural steel buildings. Chicago, Illinois, American: American Institute of Steel Construction.

Berman, J. W., Bruneau, M., & Winkley, T. (2011). Experimental investigation of self-centering steel plate shear walls. *Journal of Structural Engineering, 138*(2), 259–267.

Canadian standards association (2001). CAN/CSA-S1601. Limits states design of steel structures. Mississauga, Ontario, Canada: Canadian Standards Association.

Cao, Q., Huang, J., Wang, P., Zhang, L., Wu, D., Chen, H., & Zhang, Y. (2016). Research on failure modes and key parameters of corrugated steel shear walls. In: C. MATEC web of conferences. Shanghai, China.

Cao, Q., & Huang, J. Y. (2018). Experimental study and numerical simulation of corrugated steel plate shear walls subjected to cyclic loads. *Journal of Thin-Walled Structure, 127*, 306–317.

Dou, C., Jiang, Z.-Q., Pi, Y.-L., & Guo, Y.-L. (2016). Elastic shear buckling of sinusoidally corrugated steel plate shear wall. *Journal of Engineering Structures, 121*, 146–156.

Dou, C., Pi, Y.-L., & Gao, W. (2018). Shear resistance and post-buckling behaviour of corrugated panels in steel plate shear walls. *Journal Engineering Structures, 131*, 816–826.

Driver, R. G., Abbas, H. H., & Sause, R. (2006). Shear behaviour of corrugated web bridge girders. *Journal of the Structural Engineering. American Society of Civil Engineers, 132*, 195–203.

Easley, J. T., & Asce, M. (1969). Buckling of light-gage corrugated metal shear diaphragms. *Journal of Structural Division, 95*, 3004–3006.

Emami, F., Mofid, M., & Vafai, A. (2013). Experimental study on cyclic behaviosr of trapezoidally corrugated steel shear walls. *Engineering Structures, 48*, 750–762.

Farzampour, A., Laman, J. A., & Mofid, M. (2015). Behaviour prediction of corrugated steel plate shear walls with openings. *Journal of Constructional Steel Research, 114*, 258–268.

Gholizadeh, M., & Yadollahi, Y. (2012). Comparing steel plate shear wall behaviour with simple and corrugated plates. *Journal of Applied Mechanics and Materials, 147*, 80–85.

Hosseinzadeh, L., Mofid, M., Aziminejad, A., & Emami, F. (2017). Elastic interactive buckling strength of corrugated steel shear wall under pure shear force. *The Structural Design of Tall and Special Buildings, 26*(8), e1357.

James, M., & Manoj, M. (2001). Unstiffened steel plate shear wall performance under cyclic loading. *Journal of Structural Engineering, 127*(8), 973–974.

Kalali, H., Ghazijahani, T. G., Hajsadeghi, M., Zirakian, T., & Alaee, F. J. (2016). Numerical study on steel shear walls with sinusoidal corrugated plates. *Latin American Journal of Solids and Structures, 13*, 2502–2514.

Kalali, H., Hajsadeghi, M., Zirakian, T., & Alaee, F. J. (2015). Hysteretic performance of SPSWs with trapezoidally horizontal corrugated web-plates. *Steel & Composite Structures, 19*, 277–292.

Li, N., Zhao, Q. (2016). Experimental research on seismic behaviour of corrugated steel plate shear wall system. Dissertation, Goteborg: Department of Structural Engineering, Tianjin University.

Shon, S., Yoo, M., & Lee, S. (2017). An experimental study on the shear hysteresis and energy dissipation of the steel frame with a trapezoidal-corrugated steel plate. *Materials (basel)., 10*, 261.

Wei, Y., Tan, P., Li, Y., & Zhou, F.-L. (2015). Elastic shear buckling analysis of corrugated steel plate wall with edge stiffeners. *Journal of Earthquake Engineering and Engineer Dynamics, 35*, 200–209.

Yi, J., Gil, H., Youm, K., & Lee, H. (2008). Interactive shear buckling behaviour of trapezoidally corrugated steel webs. *Engineering Structures, 30*, 1659–1666.

Zhang, W., Mandavian, M., & Yu, C. (2018). Lateral strength and deflection of cold-formed steel shear walls using corrugated sheathing. *Journal of Constructional Steel Research, 148*(SEP), 399–408.

Zhao, Q., Sun, J., Li, Y., & Li, Z. (2017). Cyclic analyses of corrugated steel plate shear walls. *The Structural Design of Tall and Special Buildings, 26*(16), e1351.

Publisher's Note Springer Nature remains neutral with regard to jurisdictional claims in published maps and institutional affiliations.